Potential of texture-based classification in urban landscapes using multispectral aerial photos

AUTHORS:
Paidamwoyo Mhangara[1]
John Odindi[2]

AFFILIATIONS:
[1]Earth Observation, South African National Space Agency, Hartebeesthoek, South Africa
[2]School of Agricultural, Earth and Environmental Sciences, University of KwaZulu-Natal, Pietermaritzburg, South Africa

CORRESPONDENCE TO:
John Odindi

EMAIL:
Odindi@ukzn.ac.za

POSTAL ADDRESS:
School of Environmental Sciences, University of KwaZulu-Natal, Private Bag X01, Scottsville 3209, South Africa

DATES:
Received: 15 May 2012
Revised: 03 Sep. 2012
Accepted: 10 Sep. 2012

KEYWORDS:
aerial photograph; multispectral; object-based; urban; land cover

HOW TO CITE:
Mhangara P, Odindi J. Potential of texture-based classification in urban landscapes using multispectral aerial photos. S Afr J Sci. 2013;109(3/4), Art. #1273, 8 pages. http://dx.doi.org/10.1590/sajs.2013/1273

Multispectral remote sensing application in thematic urban land-use or land-cover (LULC) classification has gained popularity in the recent past. However, as a result of the complexity of urban landscapes and spectral limitations in commonly used imagery, accurate urban LULC classification has often been impeded by confusion of spectra among multiple urban LULC types. The emergence of multispectral aerial photographs, characterised by high spatial resolution and multispectral information, offers great potential for LULC classification. In this study, we hypothesised that textural information using optimum Haralick textural features inherent in multispectral aerial photographs can be used to generate reliable land-cover maps in heterogeneous urban landscapes. Haralick textural feature optimisation and object-based classification were used to discriminate diverse urban LULC types. Grey-level co-occurrence matrix (GLCM) Entropy, GLCM Mean and GLCM Angular Second Moment texture features were used to discriminate different LULC types while the Jeffreys–Matisuta separability analysis was used to identify optimum thresholds for the development of object-based classification rules. Results from object-based classification were also compared to classification output using the aerial photograph's spectral information. Results show that use of both object-based Haralick textural features and the spectral characteristics on multispectral aerial photographs can be used to generate reliable LULC classes. Classification based on object-based Haralick textural features produced higher accuracy than that based on spectral information. Multispectral aerial photographs using both object-based Haralick textural features and spectral information offer great potential in mapping urban landscapes often characterised by heterogeneous cover types.

Introduction

Generation of reliable urban land-use and land-cover (LULC) classes is critical for a better understanding and management of urban physical, ecological and social proceses.[1] In the recent past, remotely sensed data sets have become a popular data source for generation of LULC maps. Depending on the type of mission and sensor characteristics, remotely sensed data sets can be multispectral or hyperspectral with visible to microwave wavelengths, and can have a spatial resolution from sub-metres to kilometres and a temporal resolution from 30 min to several weeks.[2] Commonly, the choice of sensors for urban mapping is determined by the objective of the task, image costs and technicalities involved in image processing, analysis and interpretation.[3] Traditionally, sensors used in urban mapping include the Landsat series, Advanced Very High Resolution Radiometer (AVHRR), Quickbird, Advanced Spaceborne Thermal Emission and Reflection Radiometer (ASTHER), Airborne Visible Infrared Imaging Spectrometer and Hyperion (see Xei et al.[2] for a description of these image characteristics). Before the emergence of satellite imagery, aerial photographs played an important role in LULC mapping. However, lack of multispectral information inherent in earlier aerial photographs constrained their wide adoption for urban landscapes.[2] Recent advancement in remotely sensed data sets acquired using aerial imaging has seen an emergence of multispectral aerial photographs. This development offers invaluable potential in urban LULC mapping.

Several classification techniques are used in urban thematic feature extraction. These techniques make use of an image's pixel-by-pixel characteristics and are generally classified as 'simple' and 'advanced'. Simple classifiers include unsupervised algorithms like ISODATA and *K*-means and parametric supervised algorithms like maximum likelihood. 'Advanced' classifiers are a family of machine learning algorithms that include artificial neural networks, decision trees, support vector machines and ensembles of classifiers.[4-9]

When dealing with highly dimensional and complex LULC surfaces, machine learning algorithms have emerged as better classifiers in comparison to commonly used parametric algorithms.[10,11] However, Atkinson and Tatnall[12] and Foody[13] note that some commonly used machine learning techniques, like neural networks and support vector machines, have many parameters that need to be adjusted. Breiman[8] further notes that these techniques commonly over-fit data. Despite shortcomings related to its assumption of normal signature class distribution, highlighted for example by Swain and Davis[14], parametric algorithms using a maximum likelihood technique remain one of the most popular classifiers in use.[15-17] This classification technique is based on Bayesian decision theory and assumes a multivariate Gaussian distribution of each class and distribution.[18] Typically, this classifier depends on the statistical characteristics of image training data to generate probability density functions.[18,19]

In land-cover mapping, both textural and spectral characteristics are fundamental for object identification on aerial photographs and satellite imagery.[20,21] While the use of spectral schemes has been popular,[22] a number of researchers (e.g. Zhang and Wang[23], Haack et al.[22] and Barnsley and Barr[24]) have noted that the accuracy of LULC classifications based solely on this characteristic is often compromised by spectral similarities within and between LULC classes. Until recently, use of textural characteristics was mainly limited to visual pattern recognition and interpretation. Emerging works have, however, shown that spatial textural variations offer valuable information about structural configuration of objects and their neighbourhoods and can be used to resolve misclassification from spectral-based classes.[15,25,26] Because of their increasing availability and distinctively high spatial resolution, multispectral aerial photographs offer a great opportunity for object-based classification to complement spectral-based classification for better accuracy in urban LULC classification.

Textural feature identification and classification based on an object-oriented technique were first used in the 1970s.[27,28] However, adoption of this technique was impeded by hardware, software and image-resolution limitations.[29] In the last few decades, significant improvement in software and hardware capabilities and a proliferation of high spatial resolution remotely sensed data have increased the interest in object-oriented image analysis. These factors have also necessitated the development of more efficient and robust classification methods as an alternative to traditional per-pixel classification.[28,30] The growing popularity of object-oriented classification is largely credited to the success of Definien's eCognition software.[31]

Generally, classes in object-oriented classification are based on objects as a group of pixels instead of individual pixels. Typically, object-oriented classification starts by a segmentation process. This process is intended to partition the image into non-intersecting and internally homogeneous regions that represent surface objects on the image.[32,33] Two types of partitioning processes are commonly used: edge-based segmentation and region-based segmentation. In edge-based segmentation, boundaries are sought by detecting edges of dissimilar areas within the image and segments created by complete enclosure by edge pixels. Ultimately, pixels representing objects can either belong to a segment or form part of the segment as its boundary.[32,33] According to Geneletti[33], a major shortcoming of edge-based segmentation is that undersized surface objects are concealed by boundary pixels. On the other hand, region-based segmentation generates segments by iteratively identifying and applying homogeneity to a candidate segment. In the segmentation process, the process stops when all image pixels have been allocated a segment. A final process in object-oriented classification is the classification of objects on the entire image. This process is achieved by the allocation of objects based on training and ancillary data, shape characteristics and neighbourhood associations.[34] Typically, object-based image analysis allows for the synergy between the spatial concepts in multiscale landscape analysis, geographic information systems (GIS) and remote sensing data by providing a procedural context for effective interpretation of complex classes defined by spectral, spatial, structural and hierarchical properties.[30,31,35,36] (An extended description of object-oriented image classification can be found in Haralick and Shapiro[27], Pal and Pal[32] and Carieer et al.[37])

Object-oriented classification based on the commonly used Haralick texture analysis can be described using statistical and structural approaches.[38] This analysis has gained popularity because of its comparative calculation simplicity.[37] Originally proposed by Haralick et al.[20], Haralick textural matrices distinguish LULC surfaces based on differences in the grey levels within an image's local window. Conventionally, Haralick texture analysis is based on the determination of a grey-level co-occurrence matrix (GLCM) and grey-level difference vector (GLDV) that measure distance and angular spatial relationships over specific image sub-regions.[39] The GLCM is a matrix developed from a grey-level image that illustrates the joint probability of distribution of a pair of grey levels spaced at a specific distance and orientation while GLDV texture measures are diagonals of GLCMs.[40] Texture measures used for GLCM are also applicable in GLDV.[19] Haralick et al.[20] proposed 14 textural features that include GLCM Homogeneity, GLCM Contrast, GLCM Dissimilarity, GLCM Entropy, GLCM Angular Second Moment, GLCM Mean, GLCM Standard Deviation and GLCM Correlation.[17] Whereas the use of GLCM and GLDV textural characteristics has shown promising results on panchromatic aerial photographs and satellite imagery (e.g. Zhang et al.[41], Jensen[4] and Pu et al.[42]), the selection of textural features used is often subjective.[41,42] This often leads to a low accuracy of the output classes in urban areas commonly characterised by a high number of textural features.[43]

Comprehensive feature analysis is an important prerequisite for successful object-based classification.[44] Statistical discrimination techniques can be used to quantitatively choose features that provide the degree of statistical separability between any two classes with minimum error and features.[4,43,45] These discrimination techniques, which often are reliant on optimum features and thresholds based on probability density estimations, enable the effective selection of appropriate classification methods necessary for the attainment of high classification accuracies.[45] The transformed divergence and Jeffreys–Matisuta (JM) distance equation are among some of the most widely used for feature selection in the classification procedure.[4] Konecny[46] indicates that divergence was one of the initial statistical measures of separability still widely used for feature selection in image classification. Typically, separability or degree of divergence between two classes is computed using the mean and covariance matrices of the training sample statistics.[4] Other techniques for feature selection are based on computing the separability between two classes at a time. The Bhattacharyya distance, for instance, assumes that the two classes are Gaussian and that their means and covariance matrices are available. The JM distance is derived by applying a saturating transform to the Bhattacharyya distance.[47]

To date, urban LULC mapping using remotely sensed data has been widely successful. However, a number of challenges still persist. Foody[13] notes that LULC maps are commonly regarded as of inadequate quality operational for effective analysis and decision-making. Attempts to improve variance between LULC classes and reference data (commonly referred to as classification error) has generated a significant body of literature.[13] These efforts have been directed towards, among others, the evaluation of classification algorithms and the review of spatial, spectral and radiometric characteristics as a basis for LULC mapping.[26,44,48] In often complex urban landscapes, resolving issues related to spatial and spectral characteristics remains a challenge. In addition to interclass spectral complexity, Rodriguez-Giliano et al.[49] note that the choice of an appropriate algorithm that can handle noisy urban surface using limited training data relative to numerous urban cover types remains a challenge. According to Steele et al.[50], classification errors often arise from the classification of continuum features in discrete classes, spectra overflow of LULC types and reduced scale from ground features to a map. In line with recent efforts to solve the problems associated with classifying spectrally complex urban environments, we sought to test the feasibility of using Haralick texture to classify multispectral aerial photographs in a heterogeneous urban environment by using a rule-based object-oriented classification technique. A spectral-based classification was also performed as a reference to compare the performance of Haralick texture features against the spectral features in land-cover classification.

Methods

Data set and choice of LULC parameters

A multispectral aerial photograph within the Mowbray and Observatory suburbs of Cape Town, South Africa (Figure 1) was used in this study. The data set, acquired from the Chief Directorate: National Geo-spatial Information, has a spatial resolution of 0.5 m and a spectral resolution of four bands (sensitive to blue, green, red and near infrared regions of the electromagnetic spectrum).

The selection of surface cover types is often determined by a study's objectives, a user's needs, existing LULC types and the characteristics of photographs or imagery used.[17] In this study, we selected seven major urban classes: (1) Buildings, (2) tarred roads (subsequently referred to as 'Roads'), (3) Dense Vegetation, (4) Sparse Vegetation, (5) Grass (based on greenness density), (6) Water and (7) Bare Ground. Because of its ability to partition highly homogeneous segments at different scales simultaneously, a multiresolution segmentation algorithm was implemented to generate image object primitives. This segmentation method applies region merging algorithms that use a homogeneity criteria based on spectral and spatial information and combine local and global optimisation techniques to minimise the heterogeneity of image objects. Different scale parameters and homogeneity criteria were tested and visually assessed to evaluate the most appropriate segmentation and to avoid under-segmentation or over-segmentation (Figure 2). According to Baatz and Schäpe[51], the human eye is the most reliable and experienced source for the assessment of segmentation techniques. Consequently, a scale parameter based on visual difference was used to control the average size of image objects. We used two levels of segmentation: a shape parameter of 0.4 and a compactness parameter of 0.5. The first segmentation was at a scale parameter of 150 and the second was at a scale parameter of 50. All four spectral bands were given an equal weighting in the segmentation. A scale parameter of 150 was able to effectively segment roads and large water bodies while buildings, bare ground patches and vegetation land-cover classes (Dense Vegetation, Sparse Vegetation and Grass) could all be segmented effectively at a scale parameter of 50. Typically, multilevel segmentation

creates a hierarchical network of sub-objects (at a scale of 50) and super-objects (at a scale of 150). Object-oriented classification rules were then developed from the thresholds and spatial relationships between the multisegmentation levels.

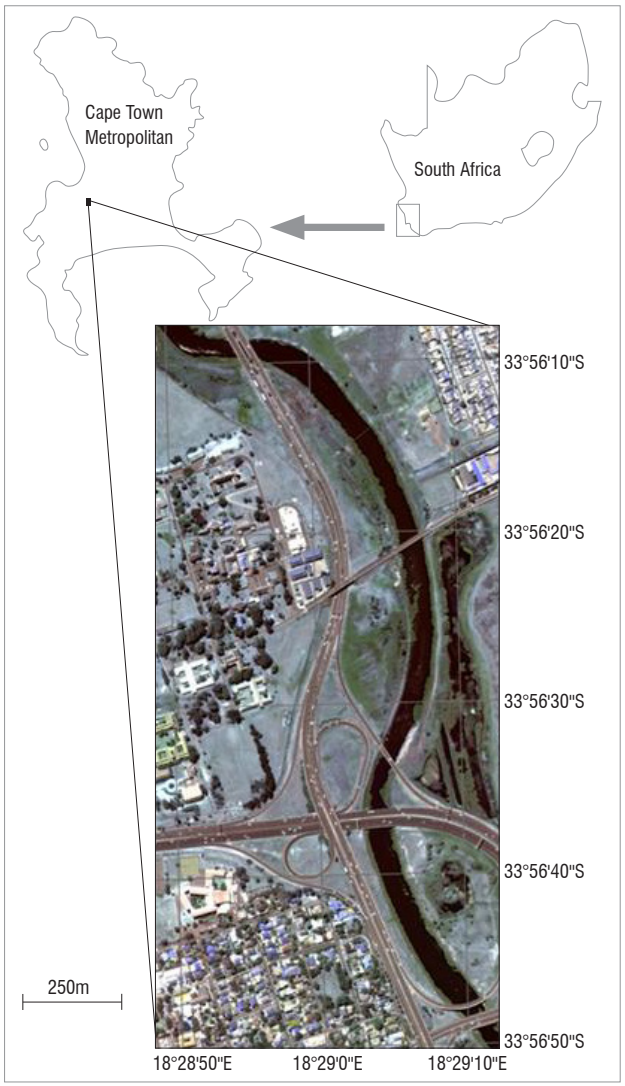

Figure 1: A map depicting the study area.

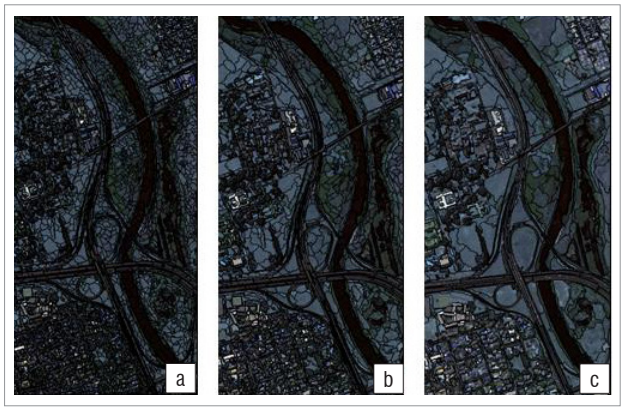

Figure 2: Image objects segmented with scale factors of (a) 30, (b) 50 and (c) 100.

The derivations of the GLCM and GLDV textural features were performed using eCognition software. To achieve directional invariance, a summation of all four directions (0°, 45°, 90° and 135°) was done before texture calculation. Commonly used texture features calculated from the GLCM and GLDV methods and adopted for this study were: Homogeneity, Angular Second Moment, Mean, Contrast, Dissimilarity, Entropy, Standard Deviation and Correlation.[13,14,16] (See Aguera et al.[17] for formulae on feature calculations.)

Spectral features such as the standard mean spectral bands, spectral indices, brightness and the standard deviation of the spectral bands were used as a reference for comparison with textural features in LULC classification. Spectral indices used in this study were the normalised difference vegetation index (NDVI), normalised difference water index (NDWI) and the bare area index (BAI). The NDVI was chosen to distinguish vegetation classes from other cover classes, NDWI to distinguish water from other cover classes and BAI to separate bare ground from green vegetation. The formulae for NDVI, NDWI and BAI are:

$$NDVI = \frac{(NIR - RED)}{(NIR + RED)} \quad \text{Equation 1}$$

$$NDWI = \frac{(GREEN - NIR)}{(GREEN + NIR)} \quad \text{Equation 2}$$

$$BAI = \frac{(BLUE - NIR)}{(BLUE + NIR)} \quad \text{Equation 3}$$

Textural and spectral features using the SEaTH algorithm

The SEaTH (SEparability and THresholds) algorithm was used to automatically identify features and thresholds and to statistically compute the separability and corresponding thresholds of object classes. SEaTH results allow an optimised object-oriented classification which minimises misclassifications by identifying optimum features with a statistical approach based on training objects. The SEaTH algorithm computes a pairwise separability of the object classes to select representative features for each object class before computing the thresholds which permit the maximum separability in the selected features.[45] SEaTH results permit rapid development of a rule-based classification model that uses statistically optimised features and thresholds compared to the trial-and-error approaches currently used in object-oriented classification. The algorithm uses the JM distance measures to compute separability between two classes on a scale from 0 to 2. The optimum threshold for the maximum separability is calculated using the Gaussian probability mixture model.

The JM distance equation was used to identify the optimum subset of textural features for the development of the classification rules. A study to evaluate four statistical measures of separability by Mausel et al.[52] notes that transformed divergence and the JM distance measures are highly correlated with classification accuracy (r=0.96 and r=0.97, respectively) while the Bhattacharyya distance and simple divergence have lower correlations. The JM is computed by applying a saturating transform to the Bhattacharyya distance (Bhat) and is expressed as:

$$JM_{cd} = \sqrt{2(1 - e^{-Bhat_{cd}})} \quad \text{Equation 4}$$

where

$$Bhat_{cd} = \frac{1}{8}(M_c - M_d)^T \left(\frac{V_c + V_d}{2}\right)^{-1} (M_c - M_d) + \frac{1}{2} \log_e \left[\frac{\left|\frac{V_c + V_d}{2}\right|}{\sqrt{(|V_c|.|V_d|)}} \right] \quad \text{Equation 5}$$

The Bhattacharyya distance assumes multivariate normality in two LULCs – *c* and *d* – and that the means M*c* and M*d* and covariance matrices V*c* and V*d* exist.[53]

Using the aforementioned SEaTH software, over 40 random objects per LULC class were selected as samples for feature analysis and threshold identification.[53] This procedure eliminates redundant GLCM textural features, minimises errors of commission and omission and expedites the identification of thresholds necessary for rule-based classification.[53]

Object-based accuracy assessment requires some modification of the traditional accuracy assessment methodology.[54] Congalton and Green[55] indicate that the number of points needed to validate the results of a classification is based on a number of criteria, such as the number of classes, and their proportion. In this study, we selected testing samples based on an overlay of at least 46 GPS points per class collected in October 2009. Homogenous land-cover objects were identified and selected from a segmented image to form the testing samples for accuracy assessment. An error matrix approach described by Congalton and Green[55] was used to assess the accuracy of object- and spectral-based LULC outputs (Tables 1 and 2).

Results

Tables 3 and 4 show that GLMC and GLDV Haralick textural features extracted from multispectral aerial photographs can be used to effectively discriminate between some urban LULC types. A comparison of the best Haralick textural feature with the highest ranked spectral features was performed as a means of evaluating the performance of Haralick textural features in LULC classification. A JM value of 2.000 suggests excellent intra-class separation, a value of 1.900 indicates good separation and a value below 1.700 indicates poor separation. The results show that some Haralick textural features are able to discriminate LULCs more effectively than spectral features. GLCM Mean Red can separate Dense Vegetation from Bare Soil more effectively than the Mean Red band alone, as revealed by a higher JM value for the GLCM Mean Red (1.996) than for the spectral Mean Red band (1.908). The discrimination between Dense Vegetation and Building was achieved more effectively by using GLCM Homogeneity, as shown by a higher JM value of 1.717, than by

Table 1: Error matrix based on training and test areas mask using Haralick textural features

User	Water	Grass	Building	Bare Ground	Dense Vegetation	Sparse Vegetation	Road	Sum
Water	115718	0	607	0	0	0	6101	122426
Grass	0	247853	25153	2154	0	947	0	276147
Building	0	0	189687	8506	0	0	9204	207397
Bare Ground	0	2401	4027	0	580	0	0	7008
Dense Vegetation	4250	2955	1409	0	145020	0	0	153634
Sparse Vegetation	4924	10108	41796	4688	0	128947	1503	191966
Road	954	0	19653	0	0	0	412164	432771
Unclassified	0	0	1268	0	0	0	0	1268
Sum	125846	263317	283600	15348	145600	129894	428972	
Accuracy								
Producer	0.919	0.941	0.668	0	0.996	0.992	0.961	
User	0.945	0.897	0.914	0	0.944	0.671	0.952	
Hellden	0.932	0.919	0.772	0	0.969	0.801	0.956	
Short	0.87	0.85	0.62	0	0.94	0.66	0.91	
KIA per class	0.911	0.926	0.611	0.001	0.995	0.991	0.943	
Overall accuracy	0.89							
KIA	0.86							

KIA, Kappa index of agreement.

Table 2: Error matrix based on training and test areas mask using spectral characteristics

User	Road	Building	Dense Vegetation	Bare Ground	Sparse Vegetation	Water	Grass	Sum
Road	418869	25779	19	0	0	13565	0	458232
Building	4121	122501	0	13457	0	0	6590	146669
Dense Vegetation	2807	1896	97299	0	5487	1138	248	108875
Bare Ground	1314	44346	0	1540	0	0	0	47200
Sparse Vegetation	1861	53907	0	391	124407	0	42303	222869
Water	0	0	2621	0	0	111143	0	113764
Grass	0	35171	45661	0	0	0	214176	295008
Unclassified	0	0	0		0	0	0	0
Sum	428972	283600	145600	15388	129894	125846	263317	
Accuracy								
Producer	0.976	0.432	0.668	0.1	0.957	0.883	0.813	
User	0.914	0.835	0.894	0.032	0.558	0.977	0.726	
Hellden	0.944	0.569	0.765	0.049	0.705	0.927	0.767	
Short	0.894	0.398	0.619	0.025	0.544	0.865	0.622	
KIA per class	0.964	0.365	0.64	0.68	0.949	0.873	0.763	
Overall accuracy	0.78							
KIA	0.73							

KIA, Kappa index of agreement.

using NDVI (1.672). GLCM Mean Green was able to separate Dense Vegetation from Grass more effectively than the spectral Mean Green band, as shown by a JM value of 1.941 for GLCM Mean Green compared with a JM value of 1.927 for the spectral Mean Green band. GLCM Mean Red and GLCM Entropy were the best Haralick textural features for discriminating between Dense Vegetation and Sparse Vegetation, shown by a higher JM value of 1.935 for GLCM Entropy compared with the JM value of 1.861 for the spectral Mean Red band.

Table 3: Separability of land-use/land-cover classes using GLCM textural features

Class combination	Feature	JM	Sign	Threshold
Dense Vegetation from Bare Ground	GLCM Mean Red	1.996	<	100.883
	GLCM Entropy	1.956	<	225.932
Dense Vegetation from Buildings	GLCM Homogeneity	1.717	<	0.022
	GLCM Mean Red	1.653	<	89.15
Dense Vegetation from Grass	GLCM Mean Green	1.941	<	95.573
	GLCM Mean Red	1.857	<	88.823
Dense Vegetation from Sparse Vegetation	GLCM Mean Red	1.935	<	86.249
	GLCM Entropy	1.935	<	86.249
Dense Vegetation from Roads	GLCM Mean NIR	1.433	>	98.319
	GLCM Mean Red	1.428	<	80.838
Dense Vegetation from Water	GLCM Mean NIR	1.876	>	62.451
	GLCM Angular Second Moment NIR	1.701	<	0.005
Roads from Bare Ground	GLCM Mean NIR	1.995	<	105.65
	GLCM Mean Red	1.937	<	115.286
	GLCM Entropy	1.937	<	115.286
Roads from Buildings	GLCM Mean NIR	1.304	<	89.891
	GLCM Mean Red	1.287	<	107.793
	GLCM Entropy	1.287	<	107.793
Roads from Grass	GLCM Mean NIR	1.938	<	99.629
	GLCM Correlation Red	1.412	<	0.835
Roads from Sparse Vegetation	GLCM Mean NIR	1.631	<	87.027
	GLCM Contrast Blue	1.279	>	22.879
Roads from Water	GLCM Mean Blue	1.992	>	64.855
	GLCM Mean Green	1.987	>	62.708
Grass from Bare Ground	GLDV Entropy	1.669	<	2.232
	GLDV Contrast /Standard Deviation	1.669	<	2.232
Grass from Buildings	GLCM Contrast	1.388	<	26.031
	GLDV Contrast	1.388	<	26.031
Grass from Sparse Vegetation	GLCM Mean NIR	1.73	>	116.6
	GLCM Mean Green	1.234	>	101.586
Grass from Water	GLCM Mean Green	2	>	68.253
	GLCM Mean Blue	1.999	>	66.129
Water from Bare Soil	GLCM Mean NIR	2	<	79.764
	GLCM Mean Red	1.999	<	70.879
	GLCM Entropy	1.999	<	70.879
Water from Buildings	GLCM Mean Red	1.853	<	58.703
	GLCM Entropy	1.853	<	58.703
Water from Sparse Vegetation	GLCM Mean Blue	2	<	71.217
	GLCM Mean Green	2	<	71.331
	GLCM Mean Red	2	<	71.331
Sparse Vegetation from Bare Ground	GLCM Mean NIR	1.921	<	118.47
	GLCM Mean Red	1.896	<	117.423
	GLCM Entropy	1.896	<	117.423
Sparse Vegetation from Buildings	GLCM Contrast Blue	1.461	<	24.844
	GLCM Contrast Green	1.452	<	26.141
Buildings from Bare Ground	GLCM Angular Second Moment Red	1.176	>	0.007
	GLCM Homogeneity	1.176	>	0.007

JM, Jeffreys–Matisuta; GLCM, grey-level co-occurrence matrix; NIR, near infrared; GLDV, grey-level difference vector.

Table 4: Separability of land-use/land-cover classes using spectral characteristics

Class combination	Feature	JM	Sign	Threshold
Dense Vegetation from Bare Ground	Mean Red	1.908	<	92.413
	Mean Green	1.782	<	91.807
Dense Vegetation from Buildings	NDVI	1.672	>	0.094
	Mean Red	1.488	<	85.926
Dense Vegetation from Grass	Mean Green	1.927	<	92.166
	Mean Red	1.925	<	89.86
Dense Vegetation from Sparse Vegetation	Mean Red	1.861	<	86.856
	NDVI	1.656	>	0.097
Dense Vegetation from Roads	NDVI	1.96	>	-0.006
	NDWI	1.949	<	0.003
Dense Vegetation from Water	Brightness	1.915	>	50.813
	BAI	1.909	<	-0.006
Roads from Bare Ground	Mean NIR	1.886	<	97.932
	BAI	1.839	>	0.008
Roads from Buildings	Mean NIR	1.277	<	89.631
	BAI	1.224	>	0.034
Roads from Grass	BAI	1.971	>	-0.03
	NDWI	1.94	>	0.011
Roads from Sparse Vegetation	BAI	1.728	>	0.018
	NDWI	1.722	>	0.043
Roads from Water	Mean Red	1.999	>	46.9
	Mean Green	1.999	>	52.938
Grass from Bare Ground	Mean Blue	1.062	<	106.561
	Standard Deviation Blue	0.989	<	6.827
Grass from Buildings	Standard Deviation Blue	1.045	<	7.205
	Standard Deviation Green	0.978	<	8.32
Grass from Sparse Vegetation	Mean NIR	1.2	>	129.669
	Brightness	1.04	>	110.757
Grass from Water	Brightness	2	>	46.9
	Mean Green	2	>	52.938
Water from Bare Ground	Mean Red	1.997	<	46.932
	Mean NIR	1.996	<	62.559
Water from Buildings	Mean Red	1.916	<	44.616
	Brightness	1.835	<	50.739
Water from Sparse Vegetation	Mean Red	2	<	50.031
	Mean Green	1.999	<	54.724
Sparse Vegetation from Bare Ground	Mean Blue	1.315	<	99.273
	Brightness	1.299	<	115.799
Sparse Vegetation from Buildings	Mean Blue	1.031	<	98.881
	Standard Deviation Blue	1.03	<	7.258
Buildings from Bare Ground	NDWI	0.326	<	0
	BAI	0.265	>	0

JM, Jeffreys–Matisuta; NDVI, normalised difference vegetation index; NDWI, normalised difference water index; BAI, bare area index; NIR, near infrared.

The GLCM NIR (near infrared) was ranked as the best feature to discriminate Roads from Bare Soil as indicated by a JM value of 1.995 compared with the value of 1.886 for the spectral Mean NIR band. GLCM Mean NIR was ranked as the most effective feature to discriminate Water from Bare Soil, with a JM value of 2.000, which was higher than the JM value of 1.997 obtained using the spectral Mean Red band. Excellent separation between Grass and Water was achieved using either the textural GLCM Mean Green or the spectral Mean Green as shown by a separability value of 2.000. Water could be discriminated effectively from Sparse Vegetation using GLCM Mean Red, GLCM Mean Green, GLCM Blue or the spectral Mean Red band as revealed by JM values of 2.000. The GLCM Mean NIR feature was ranked as the best feature to separate Sparse Vegetation from Bare Soil with a JM value of 1.921 – higher than a JM value of 1.315 achieved by the Mean Blue band which was ranked the best spectral feature. Discrimination between Grass and Sparse Vegetation was more effective using the GLCM Mean

NIR feature, with a JM value of 1.730 – higher than the low JM value of 1.200 obtained by the Mean NIR band. Although discrimination between Roads and Buildings, Grass and Bare Ground, Grass and Buildings, Sparse Vegetation and Buildings, and Buildings and Bare Ground was considerably poor (JM values below 1.700), Haralick textural features outperformed spectral features (as shown by the higher JM values obtained by Haralick textural features).

We have also shown that certain spectral features were more suitable for specific interclass separation. Mean Red or Green spectral bands could be used to effectively separate Roads from Water, as indicated by a JM value of 1.999 – higher than a separability of 1.992 for GLCM Mean Blue. The separation of Dense Vegetation from Roads could be achieved more effectively using the NDVI, as shown by a JM value of 1.960; a lower JM value of 1.433 was obtained for the same classes using the GLCM Mean NIR feature. Spectral Brightness performed better than the GLCM Mean NIR textural feature in discriminating Dense Vegetation from Water, as shown by a JM value of 1.915, higher than the JM value of 1.876 achieved by the GLCM NIR feature. The separation of Roads from Grass was more effective using the BAI spectral feature (a JM value of 1.971) than the GLCM Mean NIR textural feature (a JM value of 1.938). Roads were better discriminated from Sparse Vegetation using a BAI spectral feature (JM=1.728) than the GLCM Mean NIR textural feature (JM=1.631). The Mean Red spectral band was more effective in discriminating Water from Buildings (JM=1.916) than either the Mean GLCM Mean Red or GLCM Entropy textural features (JM=1.853).

These results demonstrate that Haralick textural features are effective in separating LULC classification with spectral similarities, such as vegetation classes with near similar spectral characteristics that often lead to spectral confusion. As shown in Figure 3, separability is more reliable using GLCM textural features than using spectral delineation.

Discussion

We have shown the feasibility of using multispectral aerial photographs with a rule-based approach and Haralick textural classification on urban landscapes. The selection of the appropriate textural features and thresholds was done objectively using the JM distance analysis. Nussbaum and Menz[53] emphasise the importance of this procedure to facilitate efficient development of LULC classification protocols. The feature analysis executed in this study ranked GLCM Mean, GLCM Second Angular Moment, GLCM Entropy, GLDV Contrast and GLCM Homogeneity as the most effective Haralick textural features for urban LULC classification. In contrast, GLCM Correlation and GLCM Standard Deviation were the least effective. These findings are consistent with Chen et al.[56] and Ozdemir et al.[57] According to Haralick et al.[20], the use of spectral and textural characteristics are important in discriminating visual elements on aerial photographs and satellite imagery. To improve the reliability of urban LULC maps, it is necessary that an integration of both parameters be considered in the classification process. Because most urban LULC units are represented by a group of pixels, object-oriented classification that takes cognisance of related pixel textural characteristics is an effective technique for heterogeneous urban landscapes.

A major limitation to textural analysis is identification of suitable textures appropriate for classification.[24] Commonly, selection of optimum thresholds for the development of classification rule is subjective. Lu and Weng [58] and Jensen[59] highlight the importance of applying suitable textures to perform reliable textural analysis. The use of the JM distance in this study facilitated the rapid selection of ideal GLCM textural features for classification. According to Jensen[59], the JM distance is a function of separability that directly relates to the final classification accuracy. Using JM, we have demonstrated the feasibility of using statistical analysis to determine appropriate thresholds for the development of classification rules.

Although we have shown the feasibility of using a rule-based object-oriented classification using Haralick textural features for urban LULC classification, spectral and ancillary information are still critical for developing better LULC protocols. Spectral information and ancillary data like Digital Surface Models can be particularly useful in resolving poor textural delineation, for example, between the Buildings and Bare Ground in this study. The optimum textural features obtained in this study may be successfully applied in other urban settings using similar multispectral aerial photography. However, the rules may not be directly transferable as a result of variability in atmospheric conditions among different areas, which requires adjustment of the classification thresholds. Considering that most urban areas comprise similar material compositions to those classified in this study, the results demonstrate that the difficulty in classifying spectral complex urban settings may be overcome by incorporating Haralick textural features. Additional contextual information would be required to further classify the broad land-cover classes derived in this study into urban sub-classes.

Accuracy of object-based classification results is still problematic as some adjustment to the per-pixel classification accuracy assessment methods is required.[54] The accuracy assessment performed in this study was a balance between attaining statistical precision and the practical

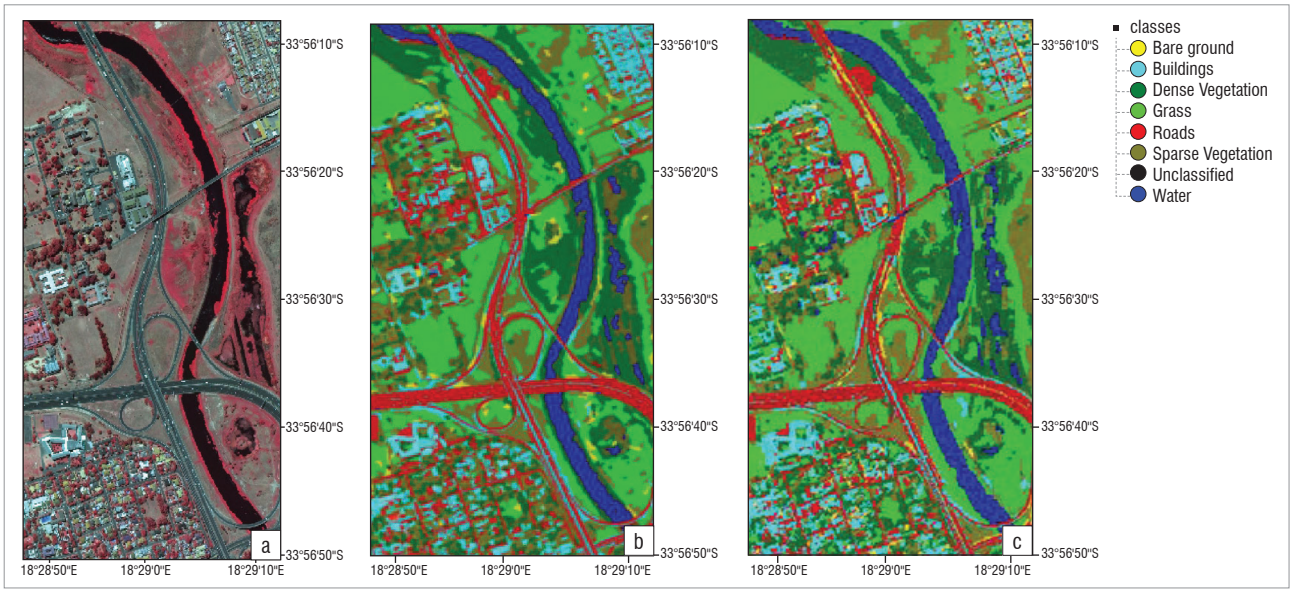

Figure 3: (a) A multispectral RGB 432 aerial photo composite, (b) a feature land-use/land-cover map using Haralick textural features and (c) a feature land-use/land-cover map using spectral characteristics.

feasibility of collecting an adequate number of representative samples – an approach which has the potential to introduce flaws.

Conclusion

The use of Haralick textures with object-based classification on multispectral aerial photographs can improve urban LULC classification. GLCM Mean, GLCM Entropy and GLCM Angular Second Moment texture features distinguished well between the different LULC classes selected in this study. Whereas high classification accuracies were achieved in this study using textural features, low separability between Buildings and Bare Ground decreased overall classification accuracy. Therefore, while the use of GLCM texture offers great potential in urban LULC classification, it does not totally resolve the heterogeneity problem in urban areas. Consequently, the integration of spectral, textural, geometric and other ancillary geographic data sets are still critical for better urban LULC accuracy. A comparison of LULC classification accuracy generated using Haralick textural features with that generated by spectral characteristics showed Haralick textural features to be superior.

Authors' contributions

P.M. collected and analysed the data and wrote the manuscript. J.O. analysed the data, wrote the manuscript and prepared it for submission.

References

1. Lu D, Mausel P, Brondizio E, Moran E. Change detection techniques. Int J Remote Sens. 2003;25(12):2365–2407. http://dx.doi.org/10.1080/0143116031000139863
2. Xie Y, Sha Z, Yu M. Remote sensing imagery in vegetation mapping: A review. J Ecol. 2008;1(1):9–23.
3. Odindi J, Mhangara P, Kakembo V. Remote sensing land-cover change in Port Elizabeth during South Africa's democratic transition. S Afr J Sci. 2012;108(5/6), Art. #886, 7 pages. http://dx.doi.org/10.4102/sajs.v108i5/6.886
4. Jensen JR. Introductory digital image processing: A remote sensing perspective. 3rd ed. Upper Saddle River, NJ: Prentice Hall; 2005.
5. Mas JF, Flores JJ. The application of artificial neural networks to the analysis of remotely sensed data. Int J Remote Sens. 2008;29(3):617–663.
6. Breiman L. Classification and regression trees. London: Chapman and Hall/CRC; 1984.
7. Mountrakis G, Im J, Ogole C. Support vector machines in remote sensing: A review. ISPRS J Photogramm. 2011;66:247–259.
8. Breiman L. Bagging predictors. Machine Learning. 1996;24(2):123–140. http://dx.doi.org/10.1007/BF00058655
9. Kotsiantis S. Supervised machine learning: A review of classification techniques. Informatica, 2007;31:249–268.
10. Huang C, Davis LS, Townshend JRG. An assessment of support vector machines for land cover classification. Int J Remote Sens. 2002;23(4):725–749. http://dx.doi.org/10.1080/01431160110040323
11. Rogan J, Miller J, Stow D, Franklin J, Levien L, Fischer C. Land cover change monitoring with classification trees using Landsat TM and ancillary data. Photogramm Eng Rem S. 2003;69(7):784–793.
12. Atkinson P, Tatnall A. Introduction neural networks in remote sensing. Int J Remote Sens. 1997;18(4):699–709. http://dx.doi.org/10.1080/014311697218700
13. Foody GM. Thematic map comparison: Evaluating the statistical significance of differences in classification accuracy. Photogramm Eng Rem S. 2004;70(5):627–633.
14. Swain PH, Davis SM. Remote sensing: The quantitative approach. New York: McGraw-Hill; 1978.
15. Gong P, Howarth PJ. Frequency-based contextual classification and grey level vector reduction for land-use identification. Photogramm Eng Rem S. 1992;58:423–437.
16. Wang L, Sousa WP, Gong P, Biging GS. Comparison of IKONOS and QuickBird images for mapping mangrove species on the Caribbean coast of Panama. Remote Sens Environ. 2004;91:432–440. http://dx.doi.org/10.1016/j.rse.2004.04.005
17. Agüera F, Aguilar FJ, Aguilar MA. Using texture analysis to improve per-pixel classification of very high resolution images for mapping plastic greenhouses. ISPRS J Photogramm. 2008;63:635–646. http://dx.doi.org/10.1016/j.isprsjprs.2008.03.003
18. Webb R. Statistical pattern recognition. 2nd ed. New York: Wiley; 2002. http://dx.doi.org/10.1002/0470854774
19. Lee JY, Warner TA. Image classification with regional based approach in high spatial resolution imagery. XXth ISPRS Congress; 2004 July 12–23; Istanbul, Turkey. London: ISPRS; 2004. p. 1–6.
20. Haralick RM, Shanmugam K, Dinstein I. Texture features for image classification. IEEE T Syst Man CYA. 1973;3(6):610–621. http://dx.doi.org/10.1109/TSMC.1973.4309314
21. Miller J, Franklin J, Aspinall R. Incorporating spatial dependence in predictive vegetation models. Ecol Model. 2007:202:225–242. http://dx.doi.org/10.1016/j.ecolmodel.2006.12.012
22. Haack B, Bryant N, Adams S. An assessment of Landsat MSS and TM data for urban and near urban land-cover digital classification. Remote Sens Environ. 1987;21:201–213. http://dx.doi.org/10.1016/0034-4257(87)90053-8
23. Zhang Q, Wang J. Texture analysis for urban spatial pattern study using SPOT imagery. IEEE T Geosci Remote. 2001;28(4):513–519.
24. Barnsley M, Barr S. Inferring urban land use from satellite sensor images using kernel-based spatial reclassification. Photogramm Eng Rem S. 1996;62:949–958. http://dx.doi.org/10.1016/j.envsoft. 2011.05.012
25. Caridade CMR, Marçal ARS, Mendonça T. The use of texture for image classification of black and white air-photographs. Int J Remote Sens. 2008;29(2):593–607. http://dx.doi.org/10.1080/014311607 01281015
26. Mather PM. Land cover classification revisited. In: Tate PM, Tate NJ, editors. Advanced remote sensing and GIS analysis. Chichester: Wiley; 1999. p. 7–16.
27. Haralick RM, Shapiro LG. Image segmentation techniques. Comput Vision Graph. 1985;29:100–132. http://dx.doi.org/10.1016/S0734-189X(85)90153-7
28. De Kok R, Schneider T, Ammer U. Object based classification application in the Alpine forest environment. In: Fusion of sensor data, knowledge sources and algorithms. Proceedings of the Joint ISPRS/Earsel Workshop; 1999 June 3–4; Valladolid, Spain. International Archives and Remote Sensing, 32 Part 7-4-3 W6.
29. Flanders D, Hall-Bayer M, Pereverzoff J. Preliminary evaluation of eCognition object based software for cut block delineation and feature extraction. Can J Remote Sens. 2003;29:441–452. http://dx.doi.org/10.5589/m03-006
30. Benz U, Hofmann P, Willhauck G, Lingenfelder I, Heynen M. Multi-resolution, object-oriented fuzzy analysis of remote sensing data for GIS-ready information. ISPRS J Photogramm. 2004;58:239–258. http://dx.doi.org/10.1016/j.isprsjprs.2003.10.002
31. Blaschke T. Object based image analysis for remote sensing. ISPRS J Photogramm. 2010;65(1):2–16. http://dx.doi.org/10.1016/j.isprsjprs.2009.06.004
32. Pal NR, Pal SK. A review on image segmentation techniques. Pattern Recogn. 1993;26:1277–1294. http://dx.doi.org/10.1016/0031-3203(93)90135-J
33. Geneletti D. A method for object-oriented land cover classification combining Landsat TM data and aerial photographs. Int J Remote Sens. 2003;24(6):1273–1286. http://dx.doi.org/10.1080/01431160210144499
34. Walter V. Object-based classification of remote sensing data for change detection. ISPRS J Photogramm. 2004;58:225–238. http://dx.doi.org/10.1016/j.isprsjprs.2003.09.007
35. Niemeyer I, Marpu PR, Nussbaum S. Change detection using object features. In: Blaschke T, Lang S, Hay GJ, editors. Object based image analysis. New York: Springer; 2008. p. 169–184. http://dx.doi.org/10.1007/978-3-540-77058-9_10
36. Gao Y, Mas J, Maathuis BH, Xiangmin Z, Van Dijk PM. Comparisons of pixel based and object oriented image classification approaches – A case study in a coal fire area, Wuda, Inner Mongolia, China. Int J Remote Sens. 2012;27(18):4039–4055.
37. Carieer AP, Debeir O, Wolff E. Assessment of very high spatial resolution satellite image segmentations. Photogramm Eng Rem S. 2005;17:1285–1294.
38. Blostein D, Ahuja N. A multi scale region detector. Comput Vision Graph. 1989;45:22–41. http://dx.doi.org/10.1016/0734-189X(89)90068-6

39. Haralick RM. Statistical and structural approaches to texture. Proc IEEE. 1979;67:786–804. http://dx.doi.org/10.1109/PROC.1979.11328

40. Smits PC, Annoni A. Upadating land-cover maps by using texture information from very high resolution space-borne imagery. IEEE T Geosci Remote. 1999;37:1244–1254. http://dx.doi.org/10.1109/36.763282

41. Zhang Q, Wang J, Gong P, Shi P. Study of urban spatial patterns from SPOT panchromatic imagery using textural analysis. Int J Remote Sens. 2003;24:4137–4160. http://dx.doi.org/10.1080/0143116031000070445

42. Pu R, Landry S, Yu Q. Object-based urban detailed land cover classification with high spatial resolution IKONOS imagery. Int J Remote Sens. 2011;32(12):3285–3308. http://dx.doi.org/10.1080/01431161003745657

43. Mathieu R, Aryal J, Chong AK. Object-based classification of IKONOS imagery for mapping large-scale vegetation communities in urban areas. Sensors. 2007;7:2860–2880. http://dx.doi.org/10.3390/s7112860

44. Nussbaum S, Niemeyer I. Canty MJ. Feature recognition in the context of automated object-oriented analysis of remote sensing data monitoring the Iranian nuclear sites. Proceedings of SPIE's Europe Symposium Optics and Photonics for Defense and Security; 2005 Oct 21. doi:10.1117/12.629581

45. Estes J, Belward A, Loveland T, Scepan J, Strahler A, Townshend J, Justice C. The way foward. Photogramm Eng Rem S. 1999:65;1089–1093.

46. Konecny G. Geoinformation: Remote sensing, photogrammetry and geographic information systems. London: Taylor and Francis; 2003. http://dx.doi.org/10.4324/9780203469644

47. Ferro CJ, Warner TA. Scale and texture in digital image classification. Photogramm Eng Rem S. 2002:68(1);51–63.

48. Foody GM. The continuum of classification fuzziness in thematic mapping. Photogramm Eng Rem S. 1999;65:443–451.

49. Rodriguez-Giliano VF, Ghimire B, Rogan J, Chica-Olmo M, Rigol-Sanchez JP. An assessment of effectiveness of a random forest classifier for land-cover classification. ISPRS J Photogramm. 2012;67:93–104. http://dx.doi.org/10.1016/j.isprsjprs.2011.11.002

50. Steele B, Winne JC, Redmond R. Estimating and mapping miscalculation probabilities for thematic land cover maps. Remote Sens Environ. 1998;66:192–202. http://dx.doi.org/10.1016/S0034-4257(98)00061-3

51. Baatz M, Schape A. Multiresolution segmentation: An optimization approach for high quality multi-scale image segmentation. In: Strobl J, editor. Proceedings of the Angewandte Geographische Informationsverarbeitung XII. Salzburg, Austria: Beiträge zum AGITSymposium; 2000. p. 12–23.

52. Mausel PW, Kramber WJ, Lee JK. Optimum band selection for supervised classification of multispectral data. Photogramm Eng Rem S. 1990;56:55–60.

53. Nussbaum S, Menz G. Object-based image analysis and treaty verification: New approaches in remote sensing applied to nuclear facilities in Iran. Heidelberg: Springer; 2008.

54. Grenier M, Labrecque S, Benoit M, Allard M. Accuracy assessment method for wetland object-based classification. In: Hay GJ, Blaschke T, Marceau D, editors. Geographic object based image analysis for the 21st Century. International Archives of the Photogrammetry, Remote Sensing and Spatial Information Sciences Vol. XXXVIII-4/C1. Calgary: University of Calgary; 2008. p. 285–289.

55. Congalton R, Green. K. Assessing the accuracy of remotely sensed data: Principles and practices. Boca Raton, FL: CRC/Lewis Press; 1999.

56. Chen D, Stow DA, Gong P. Examining the effect of spatial resolution and texture window size on classification accuracy: An urban environment case. Int J Remote Sens. 2004;25:2177–2192. http://dx.doi.org/101080/1431160310001618464

57. Ozdemir I, David A, Norton DA, Ozkan UY, Mert A, Ozdemir S. Estimation of tree size diversity using object oriented texture analysis and ASTER Imagery. Sensors. 2008;8:4709–4724. http://dx.doi.org/10.3390/s8084709

58. Lu D, Weng Q. Extraction of urban impervious surface from an IKONOS image. Int J Remote Sens. 2009;30(5):1297–1311. http://dx.doi.org/10.1080/01431160802508985

59. Jensen JR. Remote sensing of the environment: An earth resources perspective. Upper Saddle River, NJ: Prentice Hall; 2007.